Sensors and Actuators B 155 (2011) 408–414

Contents lists available at ScienceDirect

Sensors and Actuators B: Chemical

journal homepage: www.elsevier.com/locate/snb

Thin-film electrode based droplet detection for microfluidic systems

E.V. Moiseeva, A.A. Fletcher, C.K. Harnett*

University of Louisville, Department of Electrical and Computer Engineering, Louisville, KY 40208, USA

ARTICLE INFO

Article history:
Received 2 September 2010
Received in revised form 27 October 2010
Accepted 17 November 2010
Available online 24 November 2010

Keywords:
Droplet microfluidics
PDMS
Lab on chip
Droplet detection circuit

ABSTRACT

We report on a droplet-producing microfluidic system with electrical impedance-based detection. The microfluidic devices are made of polydimethylsiloxane (PDMS) and glass with thin film electrodes connected to an impedance-monitoring circuit. Immiscible fluids containing the hydrophobic and hydrophilic phases are injected with syringe pumps and spontaneously break into water-in-oil droplet trains. When a droplet passes between a pair of electrodes in a medium having different electrical conductivity, the resulting impedance change signals the presence of the particle for closed-loop feedback during processing. The circuit produces a digital pulse for input into a computer control system. The droplet detector allows estimation of a droplet's arrival time at the microfluidic chip outlet for dispensing applications. Droplet detection is required in applications that count, sort, and direct microfluidic droplets. Because of their low cost and simplicity, microelectrode-based droplet detection techniques should find applications in digital microfluidics and in three-dimensional printing technology for rapid prototyping and biotechnology.

1. Introduction

Droplet-based microfluidics has received increasing attention for applications that involve dispensing, isolating, and monitoring small amounts of reactants. Not only can the technology generate highly uniform droplets and particles using simple hardware [1], but it is also possible to perform chemical reactions and biosensing within the droplets [2,3]. The chief advantage of mixing liquids inside droplets is the lack of dispersion that occurs in continuous flow [4]. Because droplet diameter can depend on the presence of surfactants and the interfacial tension between immiscible fluids, droplet size measurement has been applied as an in-line interfacial tension sensor [5,6]. Properties like the droplet's shape, composition, volume, and location are also critical for applications in liquid dispensing and droplet-based printing. Solidified droplets are a possible route to "voxels" needed for three-dimensional (3D) printing of solid particles [7]. For printing applications, a real-time detection method is desired that offers feedback on droplet quality and arrival time so that a digital control system may coordinate movements of a stage for dispensing individual particles in registration with a substrate. Simple droplet detection systems that can be incorporated cheaply into a disposable print cartridge are likely to be commercially significant.

Detection methods originally developed for cells and particles are usually applicable to droplets. Sensing mechanisms include optical detection [8], capacitive detection [9], and impedance detection [10]. We use droplet-induced changes in electrical impedance at thin-film electrodes to detect the passage of droplets.

Optical droplet detection has been carried out in a microfluidic channel using laser light scattering and detection at a pair of optical fibers positioned across the channel [8]. This system requires a significantly more complex setup than the work here, but has advantages in performing other optics-based interrogation of the chemical environment within droplets carrying fluorescent dyes.

Because aqueous droplets generally have a different dielectric constant than the surrounding oil, capacitive detection has also been successfully demonstrated [9]. This involved building a liquid-filled capacitor from a pair of thick electrodes at the channel sidewalls, and monitoring the capacitance for changes as droplets entered and exited the electrode sandwich. While this sensitive device was able to detect changes in composition of the aqueous droplets, fabrication of the thick-film electrodes required many more steps than the method described here. The simpler thin-film electrodes are not as sensitive to droplet composition, but they are able to perform the basic droplet-counting function required by printing and dispensing applications.

2. Droplet formation and detection technique

Our system contains a T-junction microchannel system for spontaneous droplet formation in channels of 100–200 micron width and 100 micron height, and a series of three thin film electrodes located on the floor of the channel downstream from the T-junction,

* Corresponding author.
E-mail address: c0harn01@louisville.edu (C.K. Harnett).

0925-4005/$ – see front matter © 2010 Elsevier B.V. All rights reserved.
doi:10.1016/j.snb.2010.11.028

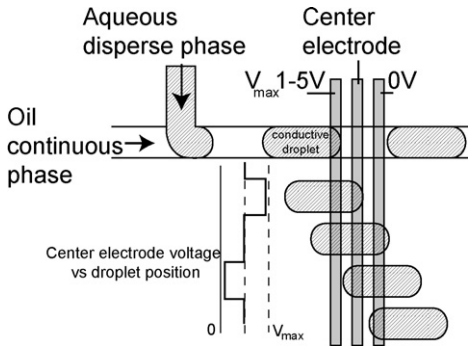

Fig. 1. Schematic of droplet formation at a T-junction and interaction of droplets with electrodes downstream. Voltages at the two outer electrodes are fixed, while voltage at the center electrode is monitored to detect droplets. The graph is a schematic of voltage at the center electrode as a droplet progresses across the three electrodes, as shown to the right of the plot.

schematically shown in Fig. 1. Electrode widths and spacings are 100 microns.

The two inlets to the T-junction are connected to syringe pumps, in which one is the oil or carrying liquid (continuous phase) and the other is the aqueous droplet liquid (dispersed phase). Droplet size and shape are determined by flow rates and channel geometry, so for printing applications it is important to understand the effect of these parameters. T-junction droplet formation spans two different regimes: the "dripping regime", which produces spherical droplets, or the "squeezing regime", which produces long plug-like droplets. This work was carried out in the plug-like "squeezing regime".

2.1. Dripping regime

When the dispersed-phase inlet channel is narrow, or when flow rates are high, small spherical droplets result. In this "dripping regime", the shear forces generated by the continuous phase, and the applied pressure from the pumps, make the head of the dispersed phase protrude into the main channel until the neck of the dispersed phase becomes thin and breaks the stream into a droplet. By altering the fluid flow rates, the channel geometry, or by changing the relative viscosity between the two phases, the frequency and size of the droplets can be varied. The diameter of the droplets in the dripping regime is determined mainly by the interfacial tension and the flow rate [8].

2.2. Squeezing regime

In contrast, when shear forces are relatively small, as seen in this work, the T-junction produces long "plugs" instead of small spherical droplets, and the droplet size is no longer determined by the interfacial tension.

The capillary number (Ca) is useful in predicting what type of droplets (if any) will be produced by a given system. It is the ratio of viscous drag forces to interfacial tension forces:

$$\mathrm{Ca} = \frac{\mu U}{\sigma} \quad (1)$$

where μ is the viscosity, U is the droplet velocity, and σ is the interfacial or surface tension between the droplet and the continuous phase. When liquids of different viscosity are used, the higher-viscosity liquid dominates the behavior of the system, and should be used in calculating Ca. A T-junction with equal inlet widths and a square channel cross section will form long plug-like droplets at Ca less than ~0.01, entering the "squeezing regime" [11]. At higher Ca, the aforementioned "dripping regime" starts: shear forces increase in importance and produce small spherical droplets (diameter smaller than the channel dimensions). For $\mathrm{Ca} \gg 1$, shear forces dominate and droplets are no longer produced; instead there are co-flowing laminar streams.

In this work, using an interfacial tension of 52 mN/m for water/hexadecane, a viscosity of 3.3 mPa s [12] (for the hexadecane continuous phase) and a flow velocity of 25 mm/s (for the fastest-moving droplets in the experiments), the maximum capillary number is 0.0016, well into the $\mathrm{Ca} < 0.01$ "squeezing" regime. Hence the droplets are plug-like and are able to span a pair of electrodes on the floor of the channel.

2.3. Droplet detection

After the plug-like droplets are formed and steady, they flow over detection electrodes approximately 5 mm downstream from the T-junction. The electrodes are monitored for changes in inter-electrode resistance due to contact with a conductive droplet. A three-electrode design allows comparison of the signal between adjacent electrode pairs; this differential mode removes background conductivity drift that occurs from temperature changes and enables amplification of the conductivity signal using a comparator circuit.

3. Device fabrication and experimental setup

3.1. Microfluidic chip fabrication

Droplet microreactors shown in Fig. 2 were fabricated in PDMS elastomer (Sylgard 184, Dow Corning) using standard soft lithography [13] on a 100 micron thick mold of SU-8 negative photoresist (MicroChem Inc).

A PDMS mold was prepared by mixing PDMS prepolymer and curing agent in a 10:1 ratio and then degassing in vacuum to remove bubbles. The degassed PDMS mixture was then distributed onto the silicon master and cured at 60 °C in an oven. After curing and demolding, holes were punched in the PDMS replica to add the fluid inlet lines.

Thin film electrodes, with widths and spacings of 100 μm, were patterned on a glass slide using photolithography. A 25–50 nm thick titanium adhesion layer was applied in a sputter deposition system followed by a 100–150 nm thick layer of platinum. Next, a perfluorodecyltrichlorosilane (FDTS) hydrophobic coating was deposited on the electrode slide using liquid precursors in a MVD100 vapor deposition system (Applied Micro Structures). The Molecular Vapor Deposition (MVD) method used has been described elsewhere [14]. The FDTS monolayer selectively adheres to the glass, producing a hydrophobic surface without significantly blocking electrical contact between electrodes and the solution. Surface cleaning and hydroxylation of the replica and a FDTS coated glass substrate were performed in an air atmosphere using a RF plasma cleaner (Harrick Plasma, 30 W, 100 mTorr) for 20 s. Substrates were then brought into contact to irreversibly bond to each other, forming a microchannel with all four walls being hydrophobic, which is necessary for maintaining aqueous droplets in an oil-based continuous phase. Wires were attached to the electrode bond pads using

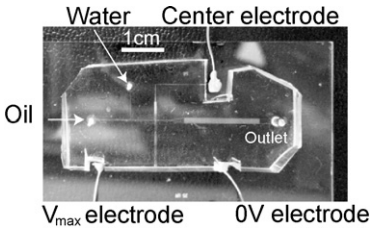

Fig. 2. Photograph of a device with T-junction and triple electrodes. Flow is from left to right.

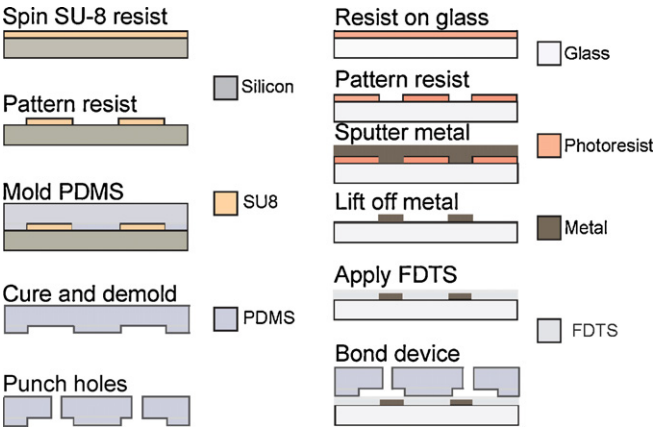

Fig. 3. Fabrication process steps for microfluidic device from PDMS. Devices are sealed to a glass slide with a self-assembled monolayer of hydrophobic FDTS.

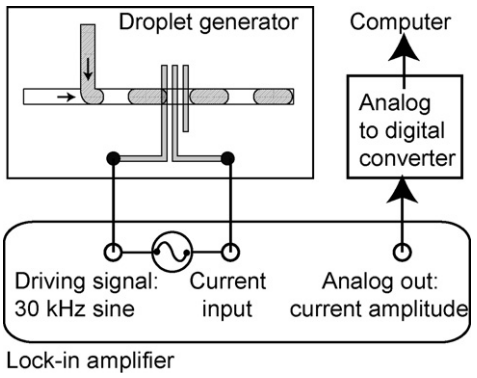

Fig. 4. Schematic of AC detection setup using SRS 830 lock-in amplifier. Two electrodes are monitored for an increase in current amplitude at 30 kHz when a conductive droplet connects them together. The third electrode is unused.

Circuit Works CW2400 conductive epoxy, Fig. 2 (left). Teflon tubing (0.030 in. OD, 0.01 in. ID, Small Parts Inc.) was press fitted into holes punched in the ports of the device, producing a liquid-tight connection. These fabrication steps are illustrated in Fig. 3.

The cross-sectional dimensions of the final assembled microfluidic channels were 100–200 μm wide × 100 μm deep.

3.2. Testing mechanism and circuit design

In our experiments, we employed aqueous droplets in n-hexadecane (viscosity of 3.34×10^{-3} Pa s). The electrical conductivity of hexadecane is very low compared to that of the aqueous droplets (<2×10^{-10} S/cm [15] vs. 1×10^{-2} S/cm for the droplets). The aqueous liquid was DI water (viscosity of approximately 10^{-3} Pa s) with 100 mM KCl added to increase the solution conductivity to the range of typical biological solutions (~10 mS/cm). In some experiments listed below, a surfactant was added by dispensing 1–3% by volume of Span-80 (sorbitan monooleate) in the hexadecane. Span-80 is known to increase the conductivity of hexadecane, but it still remains very low (4×10^{-10} S/cm for 3% Span-80 by volume) [16].

Both carrier liquid and aqueous liquid were driven by a syringe pump (KD Scientific). The working range of flow rate was 0.02–0.2 ml/h for a 1 ml Norm-Ject syringe (Henke Sass Wolf). To relate the output signal to the flow rate parameters, images of droplet formation were captured with a camera (QImaging) and an inverted microscope system (Olympus IX71). This enabled measurements of droplet size and shape. The droplets were also analyzed at the electrodes using either an AC or DC electronic signal.

3.2.1. AC amplifier method

For high-sensitivity droplet detection we used a lock-in amplifier SRS830 (Stanford Research Systems) that supplied a constant-amplitude sine wave across a single electrode pair and monitored the current, outputting a voltage directly proportional to the conductance between the electrodes. The applied signal had typical peak-to-peak amplitude of 1.1 V and frequency of 25–30 KHz. A computer data acquisition system (National Instruments USB-6009 connected to LabVIEW) sampled the lock-in output at 20 KHz, producing a time series of voltage signal as droplets flowed past the electrodes, Fig. 4.

The AC signal enabled detection of conductive droplets as well as droplets having an insulating skin around a conductive electrolyte. These high frequency signals can pass through the skin into the electrolyte by capacitive coupling. Droplets with surfactants are an example of a droplet with such an insulating skin. The main disadvantages of using this setup are price and size of equipment, and the need for two amplifiers running at different frequencies if more than one electrode pair is used. Because the current was rather large (1 μA), the high-sensitivity amplifier can be replaced by a smaller, lower-cost custom circuit board.

3.2.2. DC differential circuit

In many cases, when droplets have to merge for chemical reactions or for production of large droplets after reactants mix efficiently in small ones, surfactants are undesirable because they

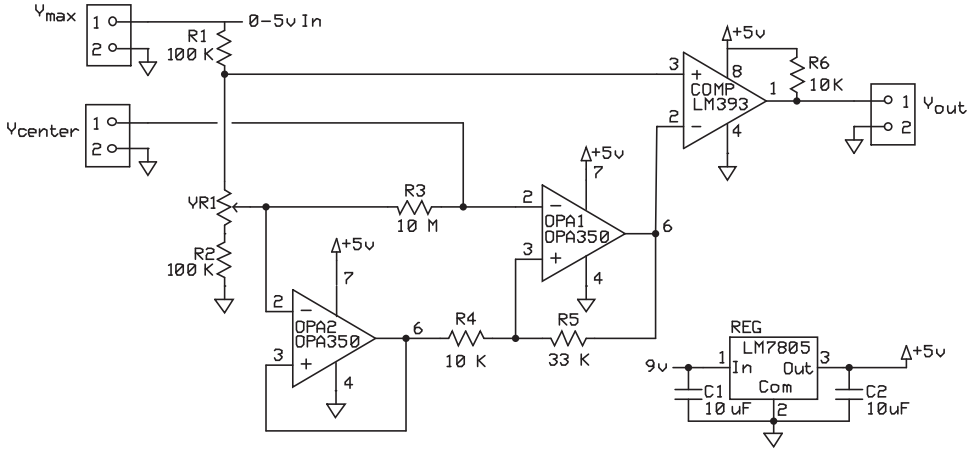

Fig. 5. Photo (left) and schematic (right) of a detection circuit to produce a digital pulse when a particle crosses electrodes.

prevent merging. Without surfactants, the droplets no longer have an insulating skin, enabling use of a much simpler and lower-cost DC experimental setup. This circuit is similar to that used to detect completion of electrochemical scanning tunneling microscope tip etching [17], where a DC current flowing in an electrolyte causes a voltage drop that is monitored using a comparator.

In the experiments, if the droplets were flowed quickly enough over the electrodes, and low voltages were used (<5 V), electrolytic gas bubbles were minimized while still maintaining a detectable faradaic current. The DC detection circuit, shown in Fig. 5, was composed of three main parts: amplifier, comparator and DC voltage source. The DC voltage source provided an adjustable voltage V_{max} (0–5 V) on the upstream electrode while the downstream electrode was held at ground. An amplifier (gain factor ~3) was connected to the middle electrode whose voltage varied as the passing conductive droplets pulled the middle voltage first toward the positive electrode, then toward the ground electrode. A comparator received the amplified signal from the middle electrode and a midpoint signal (for instance, a constant 2.5 V signal if the downstream electrode was at 5 V, shifted down or up by ~100 mV to prevent hysteresis). The circuit in Fig. 5 uses a voltage divider to create this up-shifted reference signal.

Each comparator's output consists of square wave signals which are useful for *in situ* feedback control of the droplets using a microcontroller or other digital system.

4. Results and discussion

Droplets emerge from the T-junction and cross the electrodes downstream. Typical signals of the droplets with surfactants detected using the AC amplifier method are shown in Fig. 6.

With the AC amplifier, the droplets were identified as positive pulses in the current vs. time signal. During the time the droplet was between a pair of electrodes, the electrical resistance decreased sharply. Results were approximately symmetric waveforms with a width corresponding to transit time of the entire droplet over the electrode pair, slope related to the shape of the leading and trailing edges of the droplet, and height corresponding to droplet conductivity. Similar output signal waveforms were observed for droplets without surfactant and for large and small droplets as long as those droplets spanned the minimum electrode separation.

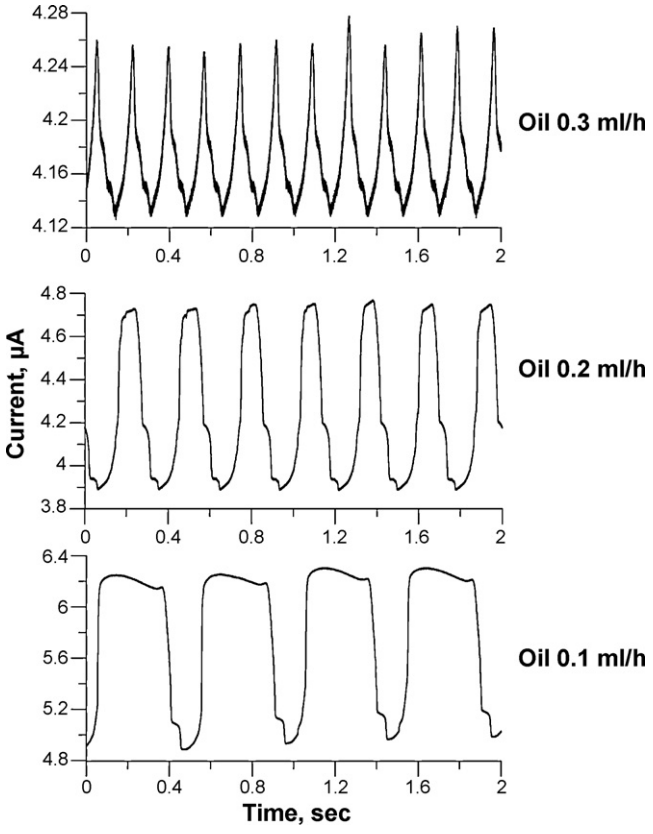

Fig. 6. Signals from lock-in amplifier at amplitude = 1.1 V, frequency = 27 kHz, flow rate of water = 0.3 ml/h, at three different oil flow rates.

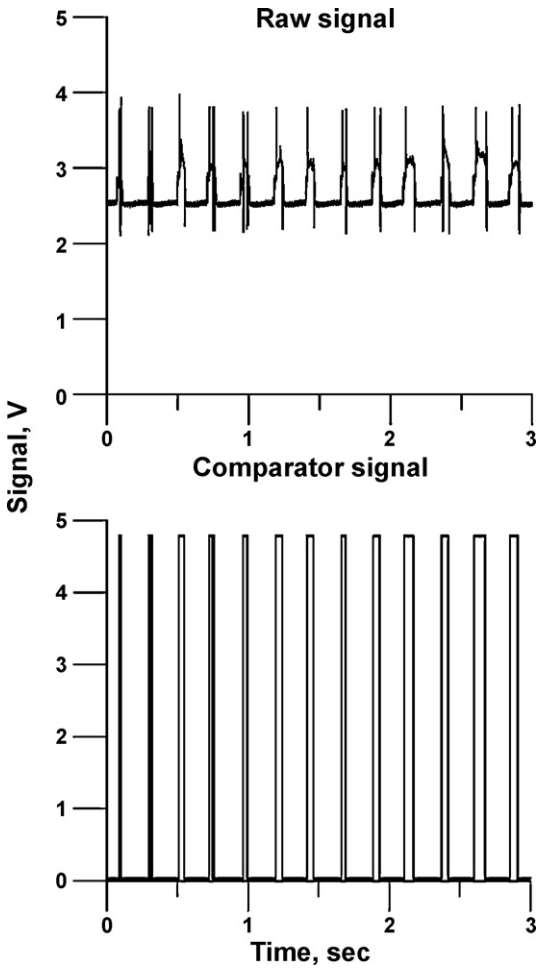

Fig. 7. Example of amplified raw signal (top) and resulting comparator signal (bottom) from center electrode.

In the case of droplets without surfactant, we also applied the DC differential method. The amplified analog data and resulting digital signal from the comparator are shown in Fig. 7, and pulse trains for different flow rates are shown in Fig. 8 along with images of the corresponding droplets in a device having a 100 × 100 micron channel.

Here the data consisted of square pulses because of the digital nature of the comparator circuit. The positive pulse width corresponded to the transit time of the *leading edge* of each conductive aqueous microdroplet as it passed from the center electrode to the downstream electrode. This is in contrast to the two-electrode AC method, where the pulse width depended on droplet length as well as speed, because the positive DC signal shuts off as the leading edge touches the third electrode. The DC pulse widths can be computed as distance/velocity:

$$Pulsewidth = \frac{d + w}{U} \quad (2)$$

where d is the insulating gap width between the first electrode pair (~100 microns), w is the electrode trace width (~100 microns), and

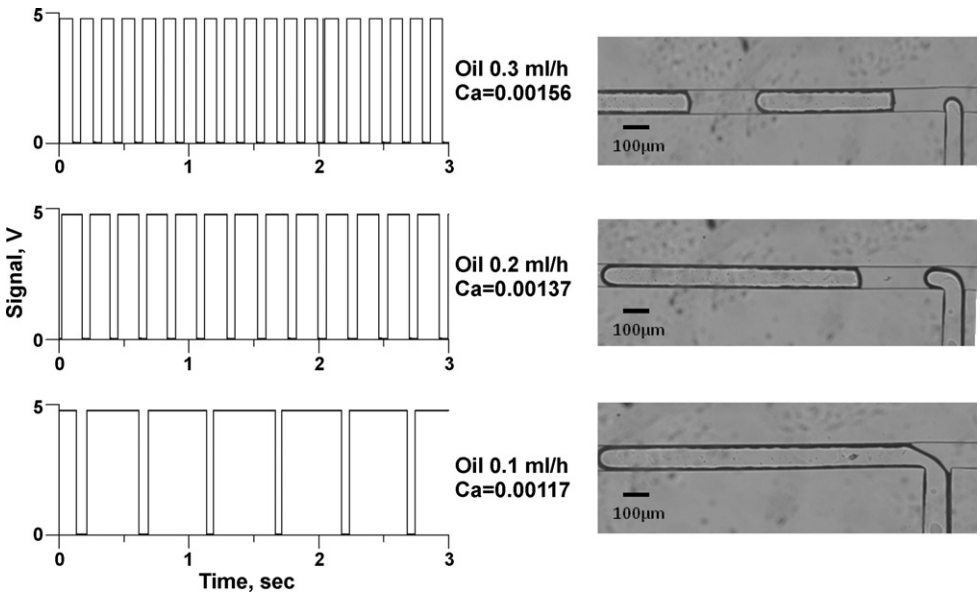

Fig. 8. (a) Digital square wave generated by the comparator that can be used for droplet control for various flow rates. (b) Photos of corresponding generated droplets with flow from right to left. Water flow rate 0.5 ml/h. Channel dimensions 100 × 100 microns.

U is the droplet velocity given by continuity:

$$U = \frac{Q_{oil} + Q_{water}}{A} \tag{3}$$

where A is the cross-sectional area of the channel, and Q_{oil} and Q_{water} are the volumetric flow rates of the oil and water.

The DC droplet detector was considerably simpler and lower cost than the AC method, but with less sensitivity to small droplets. As the droplets became smaller than the electrode spacing, pulses began to drop out and the pulse train became irregular. Therefore, experiments were run only in the plug-like regime where long droplets made contact with both electrodes during some part of their transit. Average pulse widths were computed for each set of flow rates from plots similar to those in Fig. 8. The measured pulse width data were fit to the simple model in (2) using a pair of fitting parameters a and b:

$$Pulsewidth = \frac{a}{Q_{oil} + Q_{water}} + b \tag{4}$$

By comparison with (2) and (3), the fitting parameter a should be on the order of the electrode volume, $A(d+w)$. The constant b is included to represent a shift in pulse duration induced by the additional 100 mV added to the comparator's threshold voltage to prevent hysteresis.

Fig. 9 shows how the positive pulse width decreases with an increasing flow rate of the aqueous liquid for four different flow rates of hexadecane due to the increasing velocity of the droplets. The channel was 200 microns wide and 100 microns high. The model in Eq. (4) was fit to this data by the method of least squared error, resulting in values for fitting parameter a (electrode volume) of 3.1×10^{-3} mm^3, and b (time offset) of −10 ms. The fitting parameter a is similar to the actual electrode volume of (0.1 mm + 0.1 mm) (0.2 mm × 0.1 mm) or 4×10^{-3} mm^3, and the offset time of 10 ms ranges from 5% to 50% of the pulse width. Most of the points were within one or two standard deviations of the model, as indicated by error bars. Outlying points are likely caused by imperfect hydrophobicity in the PDMS and coated glass devices. After long contact of the channels with water, the water was sometimes observed to co-flow over or under the oil, reducing the effective channel height and causing results to depart from the model. To maintain hydrophobicity, the devices should be stored in contact with air or oil, rather than water.

The pulse width can also be plotted on a log–log scale vs. total flow rate, as shown in Fig. 10. The points cluster around a line of slope −1, indicating a general dependence of pulse width on the inverse total flow rate.

Fig. 11 shows the relationship between the measured water droplet formation frequency using the DC detection circuit, and the flow rate of water for an assortment of four oil flow rates in a 200 micron wide × 100 micron tall channel. These long plug-like droplets are in the "squeezing" regime, rather than the "dripping" regime. The droplet formation frequency can be predicted by combining the total flow rate $Q_{oil} + Q_{water}$ and the droplet length L from the "squeezing" model [11]:

$$\frac{L}{w} = 1 + \alpha \frac{Q_{water}}{Q_{oil}} \tag{5}$$

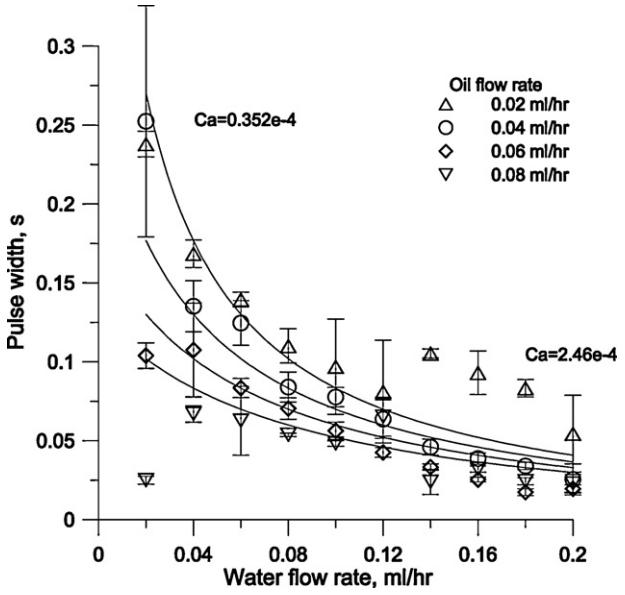

Fig. 9. Pulse width vs. water flow rate and fit to transit-time model. Channel dimensions 200 microns wide × 100 microns high.

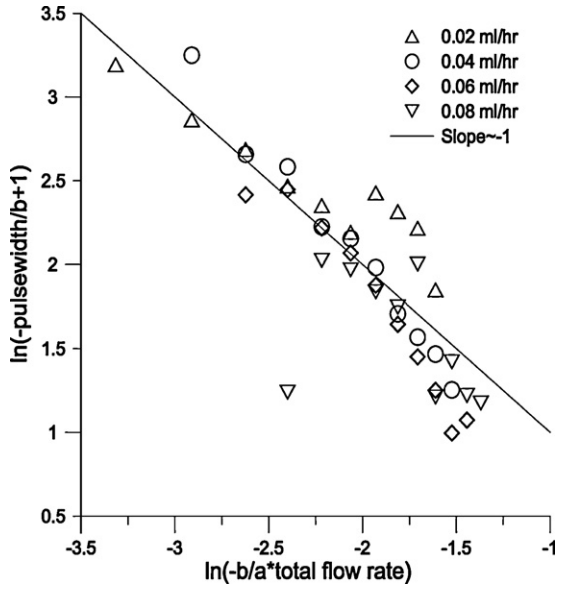

Fig. 10. Log–log plot of nondimensionalized pulse widths from Fig. 9 vs. total flow rate showing slope ~ −1.

where α is a constant on the order of 1, determined by the junction geometry, and w is the channel diameter. Notably, the squeezing model does not include the interfacial tension between the oil and water. The aqueous droplet length L is the product of the water fraction of the total flow and the distance between leading edges of successive droplets. This spacing is the droplet velocity U divided by droplet frequency f.

$$L = \frac{U}{f}\left(\frac{Q_{water}}{Q_{water} + Q_{oil}}\right) \tag{6}$$

Combining (3), (5), and (6) gives an expression for the frequency

$$f = \frac{Q_{water}}{w^3\left(1 + \alpha\frac{Q_{water}}{Q_{oil}}\right)} \tag{7}$$

The parameters w and α in (7) were fit to pulse frequency data collected from the DC circuit for four different oil flow rates and over water flow rates ranging from 0.02 to 0.2 ml/h. Fig. 11 shows this data along with the least-squares fit to (7) that gave $w = 0.22$ mm and $\alpha = 0.57$. The width parameter w is in the range of the 100–200 micron (0.1–0.2 mm) channel wall dimensions, and $\alpha = 0.57$ is on the order of 1.

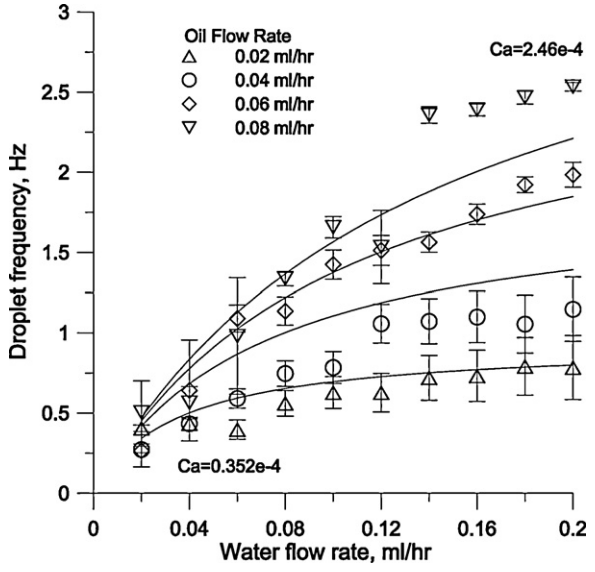

Fig. 11. Droplet frequency vs. water flow rate and fit to squeezing model. Channel dimensions 200 microns wide × 100 microns high.

5. Conclusions

We used multiphase microfluidic systems to produce droplet trains that were detected by measuring electrical impedance at thin-film electrodes downstream, and demonstrated that the resulting electrical pulse trains were consistent with the squeezing model of plug-like droplets generated at T-junctions in microfluidic chips. The low-cost DC sensing method described here applies best to long plug-like droplets. Spherical droplets could possibly be handled by elongating the droplets in a constricted channel over the electrodes, then widening the channel and allowing them to regain their spherical shape for dispensing.

Microelectrode-based sensing techniques should find several practical applications. Electrodes can apply fields for injecting, pumping and mixing fluids via electrophoresis, and for steering polarizable particles via dielectrophoresis. If thin-film electrodes are already present in the fabrication process for these purposes, the sensing electrodes can be added with little additional effort. When a droplet crosses electrodes in a medium having different electrical conductivity, the resulting impedance change signals the presence of the droplet, and a conversion circuit can then produce a digital control signal for closed-loop feedback during processing. Such feedback might build streams of droplets in a desired pattern, for instance by controlling microfluidic valves or dielectrophoretic electrodes to steer the droplets into designated downstream channels.

Acknowledgment

This work was supported by United States National Science Foundation grant 0814194, “Engineering Platforms for Exploring Cellular and Molecular Signaling Processes”.

References

[1] T. Thorsen, R.W. Roberts, F.H. Arnold, S.R. Quake, Dynamic pattern formation in a vesicle-generating microfluidic device, Phys. Rev. Lett. 86 (2001) 4163–4166.
[2] J. deMello, Control and detection of chemical reactions in microfluidic systems, Nature 442 (2006) 394–402.
[3] S.-Y. Teh, R. Lin, L.L.-H. Hung, A.P. Lee, Droplet microfluidics, Lab Chip 8 (2008) 198–220.
[4] H. Song, J.D. Tice, R.F. Ismagilov, A microfluidic system for controlling reaction networks in time, Angew. Chem. Int. Ed. 42 (2003) 768–772.
[5] N.-T. Nguyen, S. Lassemono, F.A. Chollet, C. Yang, Interfacial tension measurement with an optofluidic sensor, IEEE Sensors J. 7 (2007) 692–697.
[6] N.-T. Nguyen, S. Lassemono, F.A. Chollet, C. Yang, Microfluidic sensor for dynamic surface tension measurement, IEEE Proc. Nanobiotechnol. 153 (2006) 102–106.
[7] J. Hiller, H. Lipson, Methods of parallel voxel manipulation for 3D digital printing, in: Proceedings of the 18th Solid Freeform Fabrication Symposium, Austin TX, August, 2007, pp. 200–211.
[8] N.-T. Nguyen, S. Lassemono, F.A. Chollet, Optical detection for droplet size control in microfluidic droplet-based analysis systems, Sens. Actuators B: Chem. 117 (2006) 431–436.
[9] X. Niu, M. Zhang, S. Peng, W. Wen, P. Shang, Real-time detection, control, and sorting of microfluidic droplets, Biomicrofluidics 1 (2007) 044101.
[10] R Scott, P. Sethu, C.K. Harnett, Three-dimensional hydrodynamic focusing in a microfluidic Coulter counter, Rev. Sci. Inst. 79 (2008) 046104.
[11] P. Garstecki, M.J. Fuerstman, H.A. Stone, G.M. Whitesides, Formation of droplets and bubbles in a microfluidic T-junction—scaling and mechanism of break-up, Lab Chip 6 (2006) 438–446.
[12] J. Drelich, J.D. Miller, Spreading kinetics for low viscosity n-alkanes on a water surface as recorded by the high-speed video system, Ann. Universitatis Marie Curie-Sklodowska 54–55 (1999/2000) 105–113, Available online: www.mse.mtu.edu/~jwdrelic/ANNALES.pdf.
[13] Y.N. Xia, G.M. Whitesides, Soft lithography, Angew. Chem. Int. Ed. 37 (1998) 550–575.

[14] B. Kobrin, R.V. Fuentes, S. Dasaradhi, R. Nowak, J. Chinn, R. Ashurst, R. Maboudian, Molecular vapor deposition – a new technique for surface modification, in: Proceedings of the Eighth International Conference on Miniaturized Systems in Chemistry and Life Science, MicroTAS, vol. 1, 2004, pp. 288–290, doi:10.1039/9781847551429, Available online: http://www.rsc.org/images/uTAS2004vol1sec3_tcm18-29400.pdf.
[15] K.-Y. Li, H. Tu, A.K. Ray, Charge limits on droplets during evaporation, Langmuir 21 (2005) 3786–3794.
[16] A.S. Dukhin, P.J. Goetz, Ionic properties of so-called "non-ionic" surfactants in non-polar liquids, Newsletter 15a, Dispersion Technology Inc., Bedford Hills, NY, USA (February 2004). Available online: www.dispersion.com/pages/newsletter/articles/Newsletter15a.pdf.
[17] J.P. Ibe, P.P. Bey Jr., S.L. Brandow, R.A. Brizzolara, N.A. Burnham, D.P. DiLella, K.P. Lee, C.R.K. Marrian, R.J. Colton, On the electrochemical etching of tips for scanning tunneling microscopy, J. Vas. Sci. Technol. A8 (1990) 3570–3575.

Biographies

Evgeniya Moiseeva received B.S. and M.S. degrees in Physics from the Perm State University, Russia, in 2001 and 2003, respectively. In 2006, she received the M.S. degree from the University of Louisville, USA. Since 2007 she has been in the Ph.D. program in Electrical and Computer Engineering at University of Louisville. Her research interests include microfluidic devices, droplets, microfabrication, carbon nanotube growth and their applications.

Adrian Fletcher is currently completing undergraduate study in Electrical and Computer Engineering at the University of Louisville's Speed School of Engineering. He received a Kentucky NSF EPSCoR Research Scholars grant to fund research for data analysis and development of electronic circuits for particle detection within microfluidic devices.

C.K. Harnett is an assistant professor of Electrical and Computer Engineering at the University of Louisville. Students in the group work in the area of microfluidics, sensors and smart materials, producing new functionality through arrangements of insulators, conductors, sensors at multiple scales. After receiving a BS in physics from Harvey Mudd College (1993), and Ph.D. (2000) from Cornell University in Applied and Engineering Physics, Dr. Harnett was a postdoc at Cornell in 2000–2001 working on materials development for electron beam lithography, then on the technical staff at Sandia National Laboratories (California) in Microfluidics from 2001 to 2005.